He²⁺ HEATING VIA PARAMETRIC INSTABILITIES OF PARALLEL PROPAGATING ALFVÉN WAVES WITH AN INCOHERENT SPECTRUM

Peng He[1,2], Xinliang Gao[1,2], Quanming Lu[1,2], and Shui Wang[1,2]
[1] CAS Key Laboratory of Geospace Environment, Department of Geophysics and Planetary Science,
University of Science and Technology of China, Hefei 230026, China; gaoxl@mail.ustc.edu.cn
[2] Collaborative Innovation Center of Astronautical Science and Technology, Harbin, China
Received 2016 March 15; revised 2016 June 6; accepted 2016 June 7; published 2016 August 8

ABSTRACT

The preferential heating of heavy ions in the solar corona and solar wind has been a long-standing hot topic. In this paper we use a one-dimensional hybrid simulation model to investigate the heating of He²⁺ particles during the parametric instabilities of parallel propagating Alfvén waves with an incoherent spectrum. The evolution of the parametric instabilities has two stages and involves the heavy ion heating during the entire evolution. In the first stage, the density fluctuations are generated by the modulation of the pump Alfvén waves with a spectrum, which then results in rapid coupling with the pump Alfvén waves and the cascade of the magnetic fluctuations. In the second stage, each pump Alfvén wave decays into a forward density mode and a backward daughter Alfvén mode, which is similar to that of a monochromatic pump Alfvén wave. In both stages the perpendicular heating of He²⁺ particles occurs. This is caused by the cyclotron resonance between He²⁺ particles and the high-frequency magnetic fluctuations, whereas the Landau resonance between He²⁺ particles and the density fluctuations leads to the parallel heating of He²⁺ particles. The influence of the drift velocity between the protons and the He²⁺ particles on the heating of He²⁺ particles is also discussed in this paper.

Key words: methods: numerical – plasmas – solar wind – waves

1. INTRODUCTION

He²⁺ is the most common minor ion in the solar corona and solar wind, constituting ~4% of the total particle number density. It is typically observed to be hotter than major protons with $T_\alpha \geqslant A_\alpha T_p$ (where T_α and T_p are the temperatures of He²⁺ and protons, respectively, and A_α is the atom mass number of He²⁺), indicating the preferential heating of He²⁺ particles in the solar atmosphere (Marsch et al. 1982a, 1982b; Isenberg & Hollweg 1983; Marsch 2006; Bourouaine et al. 2013). However, until now, there has been no consensus on the physical process to account for the particle heating in the solar corona and solar wind. The possible mechanisms include the cascade of turbulence (Tu & Marsch 1995; Cranmer 2002; Hollweg & Isenberg 2002; Valentini & Veltri 2009; Valentini et al. 2010), the instabilities driven by interplanetary pick-up ions (Gray et al. 1996; Richardson et al. 1996; Li et al. 2007; Lu & Li 2007), and beam plasma (Lu et al. 2006; Gao et al. 2013). Recently, the ion acoustic waves (IAWs) and daughter Alfvén waves produced during parametric instabilities of pump Alfvén waves were found to be able to heat charged particles in the solar corona and solar wind (Araneda et al. 2008, 2009).

Alfvén waves carry most of the magnetic energy in solar coronae and solar wind, and are unstable to parametric instabilities when the compressional effect is taken into account (Galeev & Oraevskii 1963; Derby 1978; Goldstein 1978; Sakai & Sonnerup 1983; Longtin & Sonnerup 1986; Wong & Goldstein 1986; Umeki & Terasawa 1992; Hollweg 1994; Del Zanna et al. 2001; Nariyuki et al. 2007; Matteini et al. 2010). The decay instability of a monochromatic Alfvén wave in a low beta plasma was first studied by Galeev & Oraevskii (1963), where the energy of a pump Alfvén wave (k_0) was transferred to that of a forward compressible IAW (k_s) and a backward daughter Alfvén wave ($k^- = k_0 - k_s$, $k_0 < k_s$). When a two-fluid model is considered, a modulational instability can occur, which involves a forward compressible IAW (k_s) and two

forward daughter Alfvén waves ($k^\pm = k_0 \pm k_s$, $k_0 > k_s$; Sakai & Sonnerup 1983; Longtin & Sonnerup 1986; Wong & Goldstein 1986; Hollweg 1994). Furthermore, the ion kinetic effects in parametric instabilities have also been widely investigated (Terasawa et al. 1986; Inhester 1990; Vasquez 1995; Nariyuki & Hada 2006, 2007; Araneda et al. 2007; Nariyuki et al. 2007; Kauffmann & Araneda 2008), and compared with the fluid description, ion kinetic effects can reduce the instability growth rates and broaden the unstable wavenumber range.

Recently, particle dynamics during parametric instabilities have received more attention (Araneda et al. 2008, 2009; Nariyuki et al. 2009; Matteini et al. 2010; Gao et al. 2014). Araneda et al. (2008) investigated the formation of the proton beam during the modulational instability of a monochromatic Alfvén wave, which is produced by the Landau resonance between the protons and the excited IAWs. Matteini et al. (2010) found that the modulational instability and decay instability can generate a proton beam in the proton velocity distribution function, which is mainly associated with the nonlinear particle trapping. These results can provide a potential mechanism to interpret the formation of the proton velocity distribution observed in the fast solar wind, which is typically composed of a core dense and a dilute beam component (Feldman et al. 1973, 1974; Goodrich & Lazarus 1976; Marsch et al. 1982b; Goldstein et al. 2000; Tu et al. 2004).

By using a one-dimensional (1D) hybrid simulation model Araneda et al. (2009) investigated the preferential heating and acceleration of He²⁺ during the parametric instabilities of a monochromatic Alfvén wave in a proton–electron–alpha plasma, and found that He²⁺ particles can be preferentially heated in the perpendicular direction due to the transfer of the initial fluid-motion energy to random motions by the scattering mechanism, while the parallel heating of He²⁺ particles is

mainly caused by the Landau resonance between the excited IAWs and He^{2+} particles. In addition, Gao et al. (2014) used a 1D hybrid simulation and found that when the drift velocity between the protons and He^{2+} particles is sufficiently large, He^{2+} can be heated in the perpendicular direction due to the cyclotron resonance between He^{2+} particles and the cascaded high-frequency backward Alfvén waves. However, in both papers, the pump wave is assumed to be a monochromatic Alfvén wave, rather than the broad magnetic spectrum typically observed in the solar wind. In this paper, we used a 1D hybrid simulation model to investigate the heating of He^{2+} particles during the parametric instabilities of parallel propagating Alfvén waves that have an incoherent spectrum in a proton–electron–alpha plasma system. We found that the wave coupling between the Alfvén waves and the density modes resulting from the modulation (in the first stage) and the decay (in the second stage) of the initial pump Alfvén waves play an important role in heating He^{2+} particles.

The paper is composed of four sections. Simulation model and results are shown in Sections 2 and 3, respectively. In Section 4 we give conclusions and discussion.

2. SIMULATION MODEL

A 1D hybrid simulation model with periodic boundary conditions is used to investigate He^{2+} heating during the parametric instabilities of parallel propagating Alfvén waves with an incoherent spectrum in a proton–electron–alpha plasma with a low beta, where the ions (protons and He^{2+} particles) are described as particles and the electrons are treated as a massless fluid (Winske 1985). The simulations are performed along the x axis, which is parallel to the background magnetic field ($\boldsymbol{B}_0$), so all physical quantities only depend on one spatial coordinate x. For the convenience of numerical computation, the plasma density, magnetic field, and velocity are normalized by the initial uniform density ρ_0, background magnetic field $\boldsymbol{B}_0$, and background Alfvén velocity $V_A = B_0/\sqrt{\mu_0 \rho_0}$, respectively. Further, the time and space are normalized by the reciprocal of proton cyclotron frequency $\Omega_p^{-1} = m_p/e_p B_0$ (where m_p is the mass of proton and e_p is the charge of proton) and the proton inertial length c/ω_{pp} (where c is the speed of light in a vacuum and ω_{pp} is the proton plasma frequency based on the proton number density n_p), respectively.

The initial pump Alfvén waves are given as (Nariyuki et al. 2007; Matteini et al. 2010)

$$\delta \boldsymbol{B}_p = \sum_{k_0=k_1}^{k_n} \delta B_{k_0} [\cos(k_0 x - \omega_0 t + \varphi_{k_0})\hat{\boldsymbol{y}} + \sin(k_0 x - \omega_0 t + \varphi_{k_0})\hat{\boldsymbol{z}}], \quad (1)$$

$$\delta \boldsymbol{u}_i = \sum_{k_0=k_1}^{k_n} \delta u_{ik_0} [\cos(k_0 x - \omega_0 t + \varphi_{k_0})\hat{\boldsymbol{y}} + \sin(k_0 x - \omega_0 t + \varphi_{k_0})\hat{\boldsymbol{z}}], \quad (2)$$

where $\delta \boldsymbol{B}_p$ is the magnetic field fluctuation imposed by the pump Alfvén waves, and $\delta \boldsymbol{u}_i$ is the associated transverse velocity of the particles ($i = p, \alpha$, where p, α denotes the proton and He^{2+}, respectively). The initial phase φ_{k_0} is given randomly in the range $[0, 2\pi]$. From Equations (1) and (2) it is clear that the initial pump Alfvén waves are a linear superposition of parallel propagating left-handed Alfvén waves with a different wavenumber k_0. For each initial pump Alfvén

wave, the dispersion relation is derived from magnetohydro-dynamic (MHD) equations in a cold proton–electron–alpha plasma (Baumjohann & Treumann 1997):

$$\sum_{i=p,\alpha} n_i e_i \frac{(\omega_0 - U_{i0}k_0)^2}{\omega_0 - U_{i0}k_0 - \Omega_i} = -k_0^2, \quad (3)$$

where n_i is the number density, U_{i0} is the bulk velocity along the background magnetic field $\boldsymbol{B}_0$, Ω_i is the cyclotron frequency, and ω_0 and k_0 represent the frequency and wavenumber of each initial pump Alfvén wave, respectively. Moreover, δB_{k_0} and δu_{ik_0} satisfy the Walen's relation (Nariyuki et al. 2009; Matteini et al. 2010):

$$\delta u_{ik_0} = \frac{e_i}{m_i} \frac{\frac{\omega_0}{k_0} - U_{i0}}{\omega_0 - U_{i0}k_0 - \Omega_i} \delta B_{k_0}. \quad (4)$$

It is worth noting that the initial perpendicular bulk velocity of the He^{2+} particles is larger than that of the protons due to the different charge-to-mass ratios.

The particles satisfy the Maxwellian velocity distribution, and the thermal velocity of He^{2+} particles is the same as that of protons. The number of grid cells is $n_x = 600$, the size of grid cell is $\Delta x = 1.0 c/\omega_{pp}$, and the time step is $\Delta t = 0.025\Omega_p^{-1}$. The electron resistive length is set to be $L_r = \eta/\mu_0 V_A = 0.02 c/\omega_{pp}$, which is much smaller than the grid size. For each ion species, 900 macroparticles are initially evenly distributed in every grid cell. The number density of He^{2+} particles is set to be $n_\alpha/n_e = 0.04$ (where $n_e = n_p + 2n_\alpha$ is the number density of electrons). The electron beta is $\beta_e = 0.1$, while the proton beta is $\beta_p = 0.01$. The total magnetic field energy is set to be $\sum_{k_0=k_1}^{k_n} (\delta B_{k_0}/B_0)^2 = 0.04$, and the amplitude δB_{k_0} of each initial pump Alfvén wave is equal. The wavenumber k_0 of each initial pump Alfvén wave is calculated as $k_0 = \frac{2\pi m_0}{n_x \cdot \Delta x}$ (where m_0 is the mode number of wavenumber k_0), while the frequency ω_0 of each initial pump Alfvén wave can be derived from Equation (3).

3. SIMULATION RESULTS

To study the effects of the parametric instabilities of Alfvén waves with a spectrum on particle dynamics, four simulation runs (Runs 1–4) are performed in this paper. In Run 1 the initial pump wave is a monochromatic Alfvén wave with wavenumber $k_0 = 0.136$ ($m_0 = 13$) and the drift velocity between the protons and He^{2+} particles is $U_{\alpha p} = 0$. In Runs 2–4 the initial pump Alfvén waves have a spectrum with wavenumber $k_0 = 0.136, 0.157, 0.178, 0.199, 0.220, 0.241, 0.262, 0.283$ ($m_0 = 13, 15, 17, 19, 21, 23, 25, 27$) and $U_{\alpha p} = 0, 0.2, 0.5$, respectively. We first present the results of the parametric instabilities of a monochromatic Alfvén wave (Run 1). Figure 1 displays the time evolution of (a) the density fluctuations $\langle (\delta \rho/\rho_0)^2 \rangle^{1/2}$, as well as the power spectra of (b) the density fluctuations and (c) the magnetic field fluctuations for Run 1. Such a physical process has been studied in previous works (Del Zanna et al. 2001; Gao et al. 2014), where the parametric decay is found to be unstable. Here, from the figure, we see that the parametric decay occurs at about $\Omega_p t = 300$. The wavenumber of the IAW is around $k_s c/\omega_{pp} = 0.2$, while that of the backward daughter Alfvén wave propagating along the $-x$ direction is around $k^- c/\omega_{pp} = -0.06$. Therefore, the wave coupling condition $k_0 = k_s + k^-$ is almost satisfied. Several
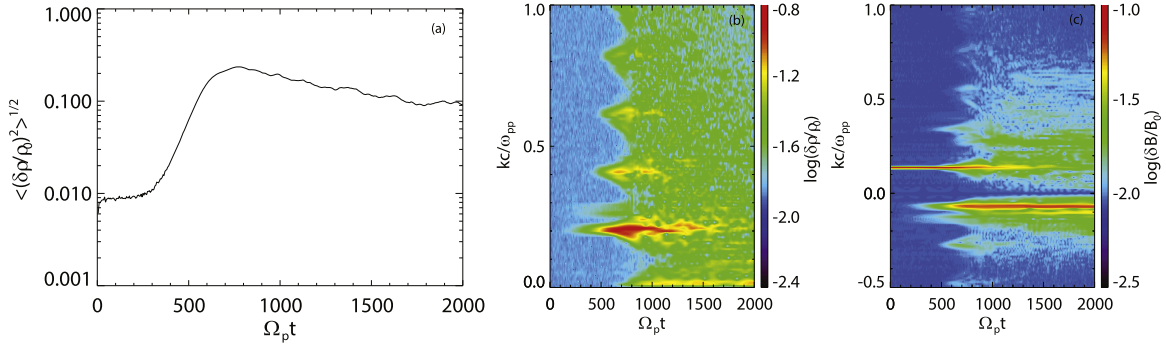
Figure 1. Time evolution of (a) the density fluctuations $\langle(\delta\rho/\rho_0)^2\rangle^{1/2}$, as well as the power spectra of (b) the density fluctuations and (c) the magnetic field fluctuations for Run 1. Here, a positive wavenumber means that the waves propagate along the $+x$ direction, and a negative one means that the waves propagate along the $-x$ direction.
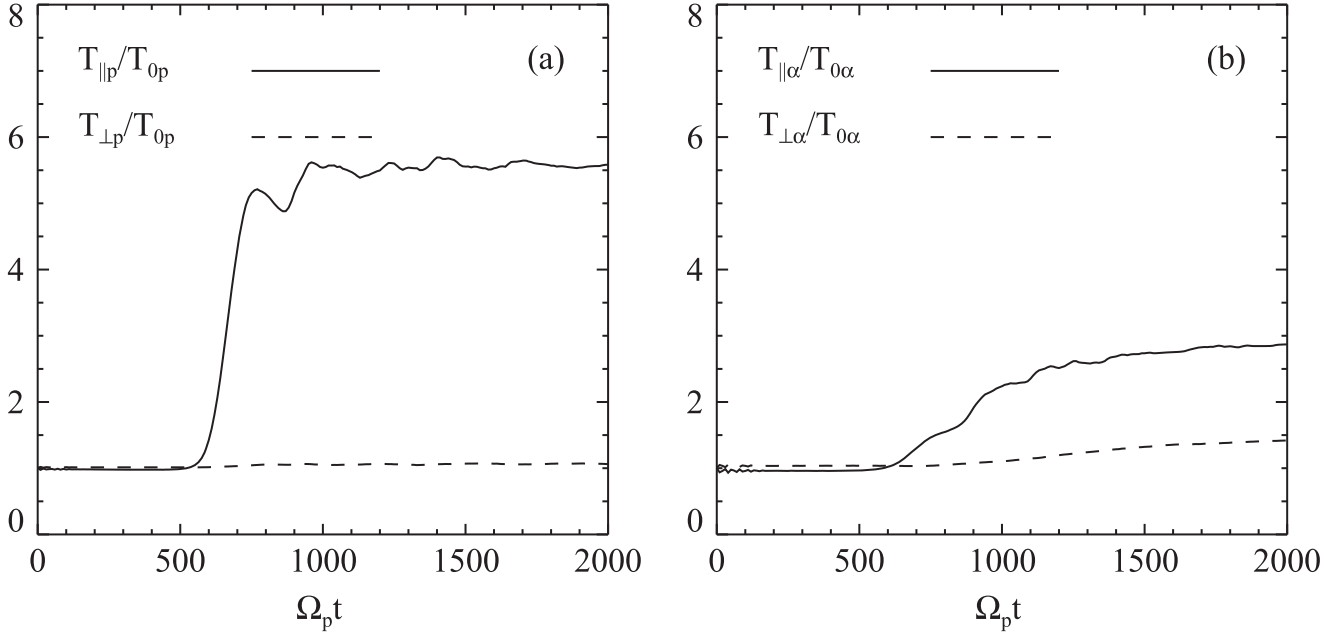

Figure 2. Time evolution of the parallel temperature (solid line) and the perpendicular temperature (dashed line) of (a) protons and (b) He^{2+} particles, respectively, for Run 1.

harmonics of the IAW are also excited after $\Omega_p t = 300$. The parametric decay saturates at about $\Omega_p t = 1100$, and the amplitude of the density fluctuations is $\langle(\delta\rho/\rho_0)^2\rangle^{1/2} \approx 0.17$.

Figure 2 plots the time evolution of the parallel and perpendicular temperatures of (a) protons and (b) He^{2+} particles for Run 1. Here, the temperatures are calculated with the following method: The parallel temperature $T_{\|i} = m_i\langle(v_x - \langle v_x\rangle)^2\rangle$ and the perpendicular temperature $T_{\perp i} = \frac{m_i}{2}\langle(v_y - \langle v_y\rangle)^2 + (v_z - \langle v_z\rangle)^2\rangle$ are calculated in every grid cell (where the bracket $\langle\bullet\rangle$ denotes an average over one grid cell), and then the final temperatures are obtained by averaging them over all grid cells. Using this type of algorithm to calculate the temperatures can eliminate the effect of the bulk velocity in each grid cell (Lu & Chen 2009; Gao et al. 2014). The parallel temperatures of both protons and He^{2+} particles increase effectively during the linear growth stage of the decay instability, which mainly results from the Landau resonance between the excited IAWs and ions (Araneda et al. 2009; Gao et al. 2014). However, there is no obvious heating in the perpendicular direction for protons or He^{2+} particles.

Runs 2–4 investigate the parametric instabilities of parallel propagating Alfvén waves with a spectrum. Figure 3 presents the time evolution of (a) the density fluctuations $\langle(\delta\rho/\rho_0)^2\rangle^{1/2}$, as well as the power spectra of (b) the density fluctuations and (c) the magnetic field fluctuations for Run 2. As shown in Figure 3(a), the amplitude of the density fluctuations increases rapidly to $\langle(\delta\rho/\rho_0)^2\rangle^{1/2} \approx 0.14$ at about $\Omega_p t = 100$, and then experiences a two-stage evolution. In the first stage (from $\Omega_p t = 0$ to about 600), the density fluctuations are caused by the modulation of the pump Alfvén waves due to the spatial inhomogeneity of the magnetic pressure (or the ponderomotive force), and then the magnetic fluctuations with a broad spectrum are generated rapidly due to the coupling between the pump Alfvén waves and density fluctuations. In the second stage (after about $\Omega_p t = 600$), each pump Alfvén wave decays into a forward density mode and a backward daughter Alfvén mode, which is similar to that of a monochromatic pump Alfvén wave.

Both the protons and He^{2+} particles can be heated during the parametric instabilities of the pump Alfvén waves with a spectrum. Figure 4 shows the scatter plots of protons in the
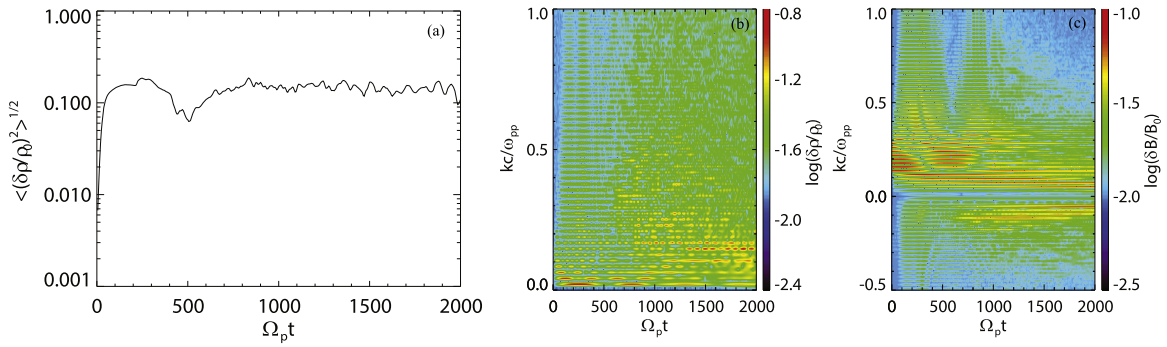
Figure 3. Time evolution of (a) the density fluctuations $\langle(\delta\rho/\rho_0)^2\rangle^{1/2}$, as well as the power spectra of (b) the density fluctuations and (c) the magnetic field fluctuations for Run 2. Here, a positive wavenumber means that the waves propagate along the $+x$ direction, and a negative one means that the waves propagate along the $-x$ direction.
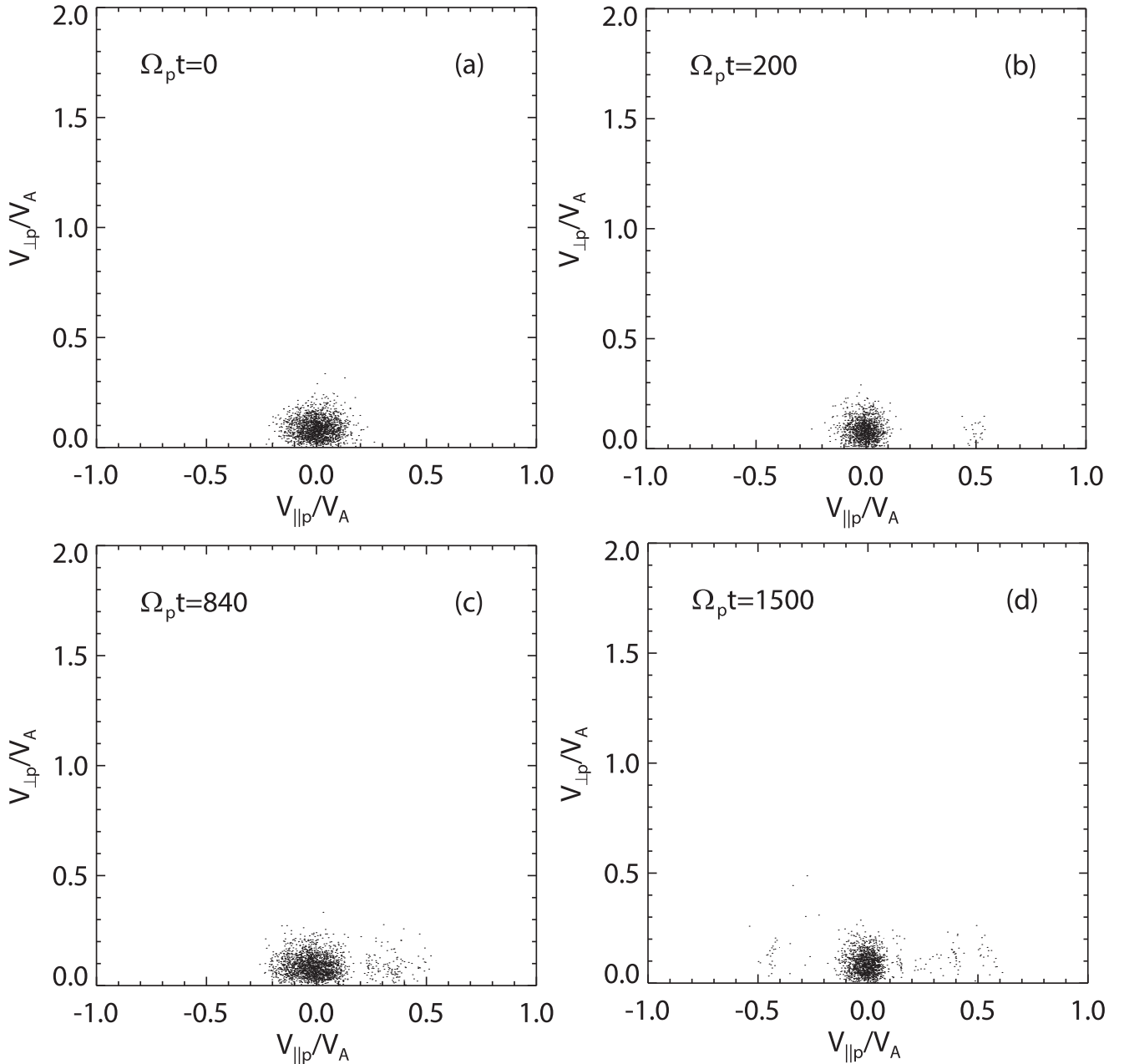

Figure 4. Scatter plots of protons in the $(v_{\|p}, v_{\perp p})$ space at (a) $\Omega_p t = 0$, (b) $\Omega_p t = 200$, (c) $\Omega_p t = 840$, and (d) $\Omega_p t = 1500$ for Run 2.
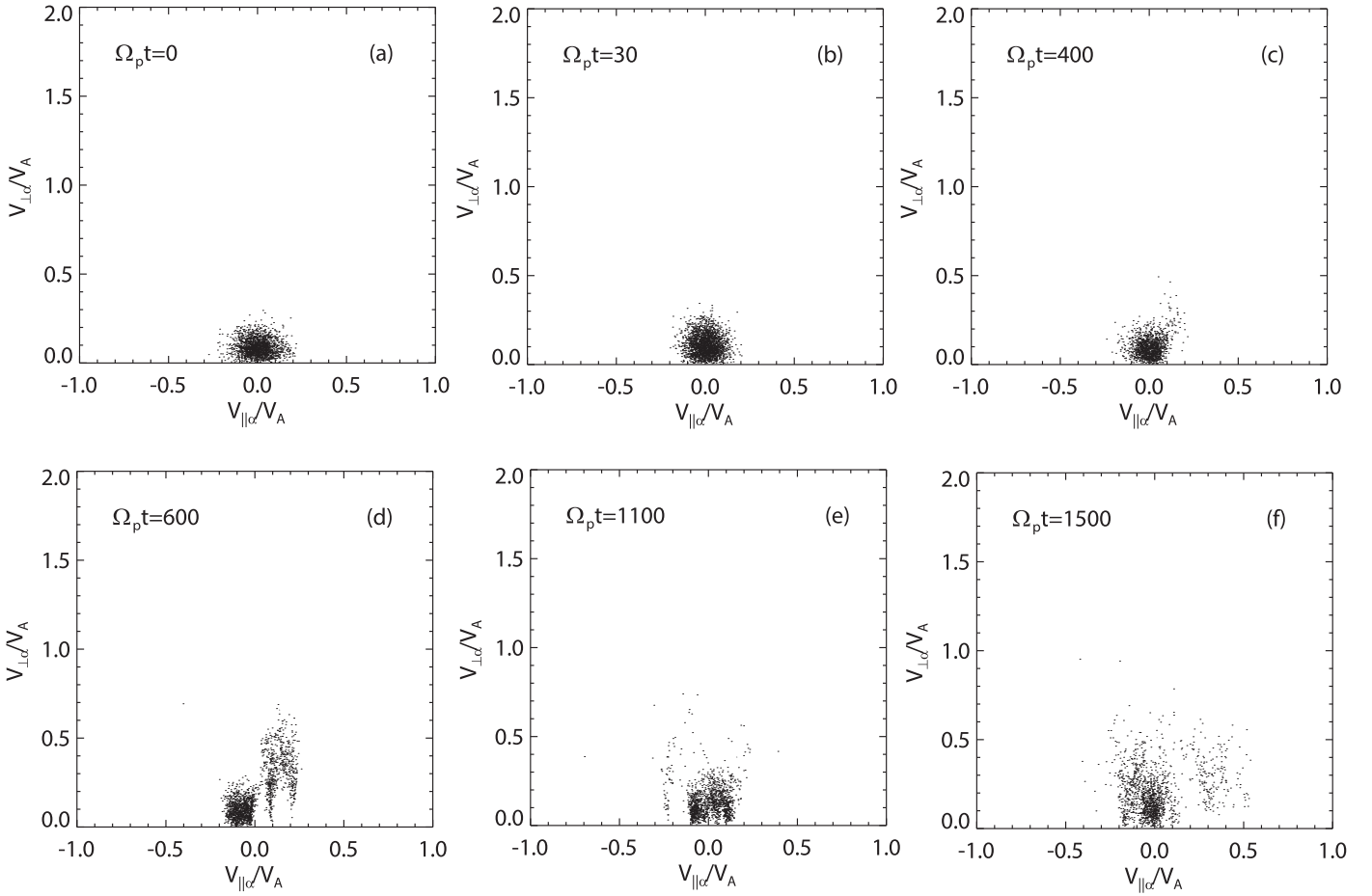
Figure 5. Scatter plots of He^{2+} particles in the $(v_{\|\alpha}, v_{\perp\alpha})$ space at (a) $\Omega_p t = 0$, (b) $\Omega_p t = 30$, (c) $\Omega_p t = 400$, (d) $\Omega_p t = 600$, (e) $\Omega_p t = 1100$, and (f) $\Omega_p t = 1500$ for Run 2.

$(v_{\|p}, v_{\perp p})$ space at (a) $\Omega_p t = 0$, (b) $\Omega_p t = 200$, (c) $\Omega_p t = 840$, and (d) $\Omega_p t = 1500$ for Run 2; Figure 5 plots the scatter plots of He^{2+} particles in the $(v_{\|\alpha}, v_{\perp\alpha})$ space at (a) $\Omega_p t = 0$, (b) $\Omega_p t = 30$, (c) $\Omega_p t = 400$, (d) $\Omega_p t = 600$, (e) $\Omega_p t = 1100$, and (f) $\Omega_p t = 1500$ for Run 2. In each panel, the particles in one fixed grid cell are recorded; the bulk velocity in each cell has already been subtracted for each particle. Initially, the protons and He^{2+} particles both satisfy the Maxwellian velocity distribution. Figure 4 shows that with the excitation of the density fluctuations, the protons can be heated in the parallel direction and form a beam-like component with the drift velocity about $0.5V_A$. Here, the parallel heating of protons is thought to be caused by the Landau resonance between the generated density modes and the protons during the parametric instabilities (Araneda et al. 2008, 2009; Gao et al. 2014). However, due to the dispersion of the density modes, the parallel heating of protons and the formation of the beam component are less efficient when compared with that during the modulation or decay instability of a monochromatic pump Alfvén wave.

Moreover, as shown in Figure 5, He^{2+} particles can be heated not only in the parallel direction, but also in the perpendicular direction, which is quite different from that of the monochromatic pump Alfvén wave displayed in Figure 2. Here, He^{2+} particles interact with the density modes through the Landau resonance in the parallel direction just like protons, while He^{2+} particles are also heated in the perpendicular direction through the cyclotron resonance with the cascaded high-frequency magnetic fluctuations. It is worth noting that the perpendicular heating of He^{2+} particles starts very early, just after the generation of higher-frequency magnetic fluctuations in the first stage. Figure 6 shows the time evolution of the parallel and perpendicular temperatures of (a) protons and (b) He^{2+} particles, respectively, for Run 2. The protons can be heated only in the parallel direction, but with a little lower efficiency compared with that shown in Figure 2(a) for Run 1. Furthermore, in addition to parallel heating, He^{2+} particles can also be effectively heated in the perpendicular direction, which was not observed in Figure 2(b) for Run 1.

We also investigate the effects of the drift velocity between the protons and He^{2+} particles on the heating of He^{2+} particles during the parametric instabilities of the pump Alfvén waves with a spectrum. Figure 7 shows the time evolution of (a) the parallel temperature and (b) the perpendicular temperature of He^{2+} particles for different drift velocities $U_{\alpha p} = 0$, $0.2V_A$, $0.5V_A$. The increase of the parallel temperature is mainly due to the Landau resonance between the density modes and He^{2+} particles; the phase velocity of the density modes is about $0.5V_A$. Therefore, the parallel heating of He^{2+} particles is most efficient when the drift velocity is about $0.5V_A$, and it becomes more efficient as the drift velocity increases, as shown in Figure 7(a). But if we increase the drift velocity further, the efficiency of the parallel heating decreases (not shown).
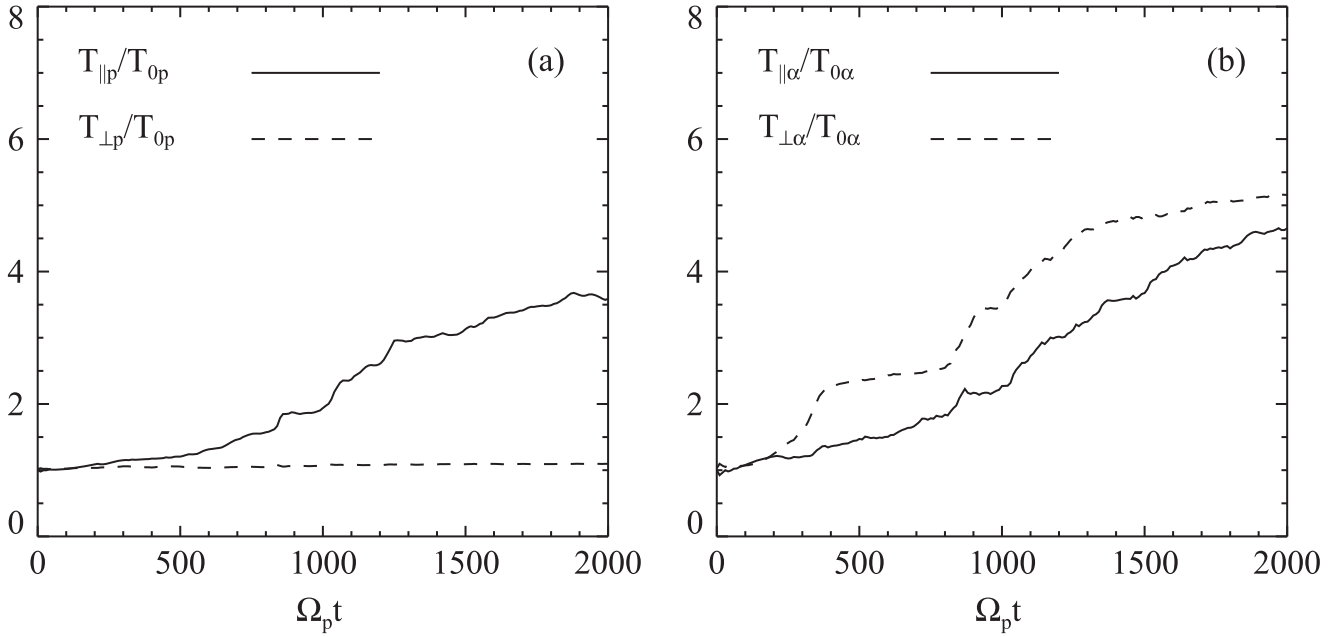
Figure 6. Time evolution of the parallel temperature (solid line) and the perpendicular temperature (dashed line) of (a) protons and (b) He^{2+} particles, respectively, for Run 2.
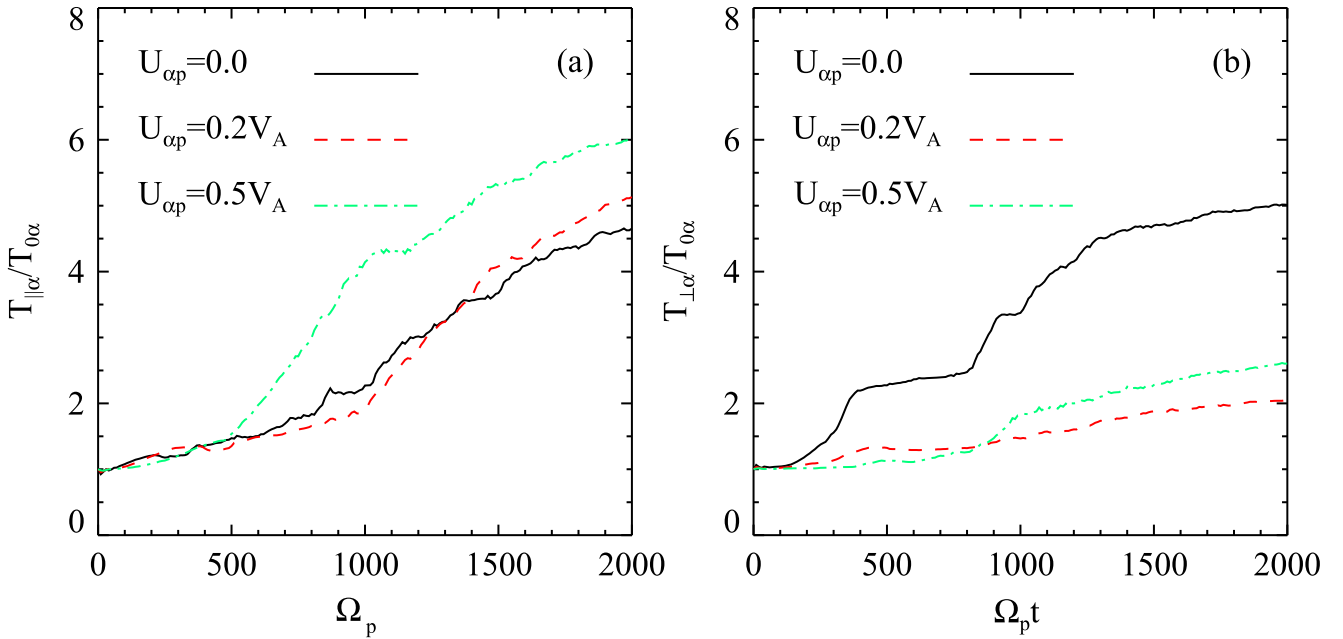

Figure 7. Time evolution of (a) the parallel temperature and (b) the perpendicular temperature of He^{2+} particles for different drift velocities between the protons and He^{2+} particles. The results for the drift velocities $U_{\alpha p} = 0$, $0.2V_A$, $0.5V_A$ are denoted by the black solid, red dashed, and green dot-dashed lines, respectively.

However, Figure 7(b) shows that the perpendicular temperature of He^{2+} particles decreases with the increase of the drift velocity. The perpendicular heating of He^{2+} particles is mainly the result of the cyclotron resonance with the excited forward magnetic fluctuations that have frequencies around $0.5\Omega_p$. When the drift velocity of the He^{2+} particles increases, the main He^{2+} particles will start becoming resonant with the magnetic fluctuations with higher frequencies. As displayed in Figure 3(c), the amplitude of the magnetic fluctuations decreases as frequency increases. Therefore, the decreasing perpendicular heating efficiency of He^{2+} particles as the drift velocity increases, can be easily understood.

4. CONCLUSIONS AND DISCUSSION

In this paper the 1D hybrid simulation model is used to study the heating of He^{2+} particles via the parametric instabilities of parallel propagating Alfvén waves with an incoherent spectrum in a proton–electron–alpha plasma system. The evolution of the parametric instabilities has two different stages. In the first stage, density fluctuations are generated due to the envelope modulation of the initial pump Alfvén waves, and then the high-frequency magnetic fluctuations are produced rapidly due to the coupling between the density modes and the pump Alfvén modes. In the second stage, each pump Alfvén wave decays into a forward density mode and a backward daughter

Alfvén mode, which is similar to that of a monochromatic pump Alfvén wave. In both stages, He^{2+} particles can resonantly interact with the high-frequency magnetic fluctuations and be efficiently heated in the perpendicular direction, whereas the Landau resonance due to the exited density modes can lead to the parallel heating of He^{2+} particles. With the increase of the drift velocity between the protons and He^{2+} particles, the parallel heating of He^{2+} becomes more efficient, while the perpendicular heating tends to be less efficient.

Gao et al. (2014) also studied the heating of He^{2+} particles during the parametric instabilities of a monochromatic parallel propagating pump Alfvén wave. At first, it decays into a forward IAW and a backward daughter Alfvén wave. Then, the backward daughter Alfvén waves can be cascaded toward higher frequencies due to the modulational instability. Finally, the resulting high-frequency waves can heat He^{2+} particles due to the cyclotron resonance. This heating mechanism requires the drift velocity between the protons and He^{2+} particles to be sufficiently large ($\sim V_A$), and it also takes long time for daughter waves to be fully developed. However, the drift velocity of He^{2+} particles does not meet this requirement in most real-life situations, especially for the solar wind and solar corona. Moreover, they initialize the simulation model with a monochromatic Alfvén wave, which is different from the broad magnetic spectrum typically observed in the solar wind.

Both Nariyuki et al. (2010) and Maneva et al. (2013) also investigated the heating of He^{2+} particles during parametric instabilities of the incoherent magnetic spectrum, but they attributed the perpendicular heating of He^{2+} particles in large part to the non-resonant pitch angle scattering. However, we clearly observe the higher-frequency magnetic fluctuations resulting from the couplings between the density modes and the magnetic modes in Figure 3(c), which then results in the perpendicular heating of He^{2+} particles through the cyclotron resonance. This is supported by comparison with the results of the monochromatic Alfvén wave for Run 1, where the higher-frequency magnetic fluctuations are quite weak, and no obvious enhancement of the perpendicular temperature of He^{2+} particles is observed (Figure 2(b)). The definition of temperature in this study is also different from the "apparent temperature" used in previous works (Araneda et al. 2009; Nariyuki et al. 2010; Maneva et al. 2013), which contain both thermal and bulk (larger than thermal velocity) velocities. This is a possible reason that no remarkable enhancement ($<50\%$ of the initial temperature) of the perpendicular temperature of He^{2+} particles was found in previous works. According to Kauffmann & Araneda (2008), the existence of He^{2+} particles can introduce extra modes (alpha sound modes), which can also couple with the magnetic modes leading to higher-frequency magnetic fluctuations. In the present study, the parallel heating of both protons and He^{2+} particles is also caused by the Landau resonance (Araneda et al. 2008, 2009) with the excited IAWs during the parametric instabilities; the perpendicular heating of He^{2+} particles is mainly due to the cyclotron resonance with the higher-frequency magnetic fluctuations. In the first stage, the density fluctuations are easily generated by the envelope modulation of the initial pump Alfvén waves, which are then coupled with the pump Alfvén modes to produce the higher-frequency magnetic fluctuations. In the second stage the density modes generated by the parametric decay can also be involved in the cascade of the magnetic energy into the higher-frequency magnetic modes. Comparing Figures 3(c) and 6(b),

we see that the enhancement of the perpendicular temperature of the He^{2+} particles is closely correlated with the excitation of high wavenumber (high-frequency) magnetic fluctuations. The cyclotron resonance interactions with He^{2+} particles are also shown in Figure 5. To further show the role of parametric instability in the heating process, we performed another run that was nearly same as Run 2, but with a large electron beta $\beta_e = 2.0$ (not shown here). In the second stage, the parametric decay is severely quenched due to the high plasma beta. As a result, the density fluctuations become much weaker, which then only results in much weaker coupling with the magnetic modes. Ultimately, in the second stage there are no strong high wavenumber magnetic fluctuations and no further enhancement of the perpendicular heating of He^{2+} particles. The dependence of the perpendicular heating on the relative velocity between the protons and He^{2+} particles illustrated in Figure 7 can be easily understood based on this heating mechanism. When the drift velocity of He^{2+} particles increases, the frequency of the magnetic modes resonant with He^{2+} particles will also increase. Meanwhile, the amplitude of the magnetic modes decreases rapidly with the increase of the frequency, therefore the perpendicular heating becomes less efficient with the increase of the drift velocity. However, when the drift velocity of He^{2+} particles is sufficiently large ($\geqslant 0.5\ V_A$), the generated backward daughter Alfvén waves during the parametric decay (in the second stage) will resonantly heat He^{2+} particles (Gao et al. 2014).

In situ measurements of the solar wind and remote sensing observations of the solar corona have revealed that the minor heavy ions are preferentially heated over the protons (Feldman et al. 1974; Marsch et al. 1982a, 1982b; Kohl et al. 1998; Li et al. 1998; Marsch 2006; Von Steiger & Zurbuchen 2006). The dissipation of Alfvén waves is commonly believed to be related to the preferential heating of the heavy ions. Our simulations have shown that the high-frequency magnetic fluctuations, which are generated due to the couplings between the density modes and the magnetic modes during the parametric instabilities, can resonantly heat the minor heavy ions efficiently, and the heating efficiency will be enhanced with the decrease of the drift velocity between the minor heavy ions and the protons. Our results may provide a possible explanation for the preferential heating of the minor heavy ions observed in the solar wind and solar corona.

REFERENCES

Araneda, J. A., Maneva, Y., & Marsch, E. 2009, PhRvL, 102, 175001
Araneda, J. A., Marsch, E., & Vinas, A. F. 2007, JGR, 112, A04104
Araneda, J. A., Marsch, E., & Vinas, A. F. 2008, PhRvL, 100, 125003
Baumjohann, W., & Treumann, R. A. 1997, Basic Space Plasma Physics (London: Imperial College Press)
Bourouaine, S., Verscharen, D., Chandran, B. D. G., Maruca, B. A., & Kasper, J. C. 2013, ApJL, 777, L3
Cranmer, S. R. 2002, SpSR, 101, 229
Del Zanna, L., Velli, M., & Londrillo, P. 2001, A&A, 367, 705
Derby, N. F. 1978, ApJ, 224, 1013
Feldman, W. C., Asbridge, J. R., Bame, S. J., & Montgome, M. D. 1973, JGR, 78, 2017
Feldman, W. C., Asbridge, J. R., Bame, S. J., & Montgomery, M. D. 1974, RvGeo, 12, 715

Galeev, A. A., & Oraevskii, V. N. 1963, SPhD, 7, 998
Gao, X., Lu, Q., Li, X., et al. 2014, ApJ, 780, 56
Gao, X. L., Lu, Q. M., Li, X., Shan, L. C., & Wang, S. 2013, ApJ, 764, 71
Goldstein, B. E., Neugebauer, M., Zhang, L. D., & Gary, S. P. 2000, GeoRL, 27, 53
Goldstein, M. L. 1978, ApJ, 219, 700
Goodrich, C. C., & Lazarus, A. J. 1976, JGR, 81, 2750
Gray, P. C., Smith, C. W., Matthaeus, W. H., & Otani, N. F. 1996, GeoRL, 23, 113
Hollweg, J. V. 1994, JGR, 99, 23431
Hollweg, J. V., & Isenberg, P. A. 2002, JGR, 107, 1147
Inhester, B. 1990, JGR, 95, 10525
Isenberg, P. A., & Hollweg, J. V. 1983, JGR, 88, 3923
Kauffmann, K., & Araneda, J. A. 2008, PhPl, 15, 062106
Kohl, J. L., Noci, G., Antonucci, E., et al. 1998, ApJL, 501, L127
Li, X., Habbal, S. R., Kohl, J. L., & Noci, G. 1998, ApJL, 501, L133
Li, X., Lu, Q. M., & Li, B. 2007, ApJL, 661, L105
Longtin, M., & Sonnerup, B. U. O. 1986, JGR, 91, 6816
Lu, Q. M., & Chen, L. 2009, ApJ, 704, 743
Lu, Q. M., & Li, X. 2007, PhPl, 14, 042303
Lu, Q. M., Xia, L. D., & Wang, S. 2006, JGR, 111, 9101
Maneva, Y. G., Vinas, A. F., & Ofman, L. 2013, JGR, 118, 2842

Marsch, E. 2006, LRSP, 3, 1
Marsch, E., Muhlhauser, K. H., Rosenbauer, H., Schwenn, R., & Neubauer, F. M. 1982a, JGR, 87, 35
Marsch, E., Muhlhauser, K. H., Schwenn, R., et al. 1982b, JGR, 87, 52
Matteini, L., Landi, S., Velli, M., & Hellinger, P. 2010, JGR, 115, A09106
Nariyuki, Y., & Hada, T. 2006, PhPl, 13, 124501
Nariyuki, Y., & Hada, T. 2007, JGR, 112, A10107
Nariyuki, Y., Hada, T., & Tsubouchi, K. 2007, PhPl, 14, 122110
Nariyuki, Y., Hada, T., & Tsubouchi, K. 2009, JGR, 114, A07102
Nariyuki, Y., Hada, T., & Tsubouchi, K. 2010, PhPl, 17, 072301
Richardson, J. D., Phillips, J. L., Smith, C. W., & Gray, P. C. 1996, GeoRL, 23, 3259
Sakai, J. I., & Sonnerup, B. U. O. 1983, JGR, 88, 9069
Terasawa, T., Hoshino, M., Sakai, J. I., & Hada, T. 1986, JGR, 91, 4171
Tu, C. Y., & Marsch, E. 1995, SSRv, 73, 1
Tu, C. Y., Marsch, E., & Qin, Z. R. 2004, JGR, 109, A05101
Umeki, H., & Terasawa, T. 1992, JGR, 97, 3113
Valentini, F., Califano, F., & Veltri, P. 2010, PhRvL, 104, 205002
Valentini, F., & Veltri, P. 2009, PhRvL, 102, 225001
Vasquez, B. J. 1995, GR, 100, 1779
Von Steiger, R., & Zurbuchen, T. H. 2006, GeoRL, 33, L09103
Winske, D. 1985, SSRv, 42, 53
Wong, H. K., & Goldstein, M. L. 1986, JGR, 91, 5617